

# Affordable, entropy-consistent Euler flux functions II: Entropy production at shocks

Farzad Ismail<sup>a,\*</sup>, Philip L. Roe<sup>b</sup>

<sup>a</sup>School of Aerospace Engineering, Universiti Sains Malaysia, 14300 Pulau Pinang, Malaysia

<sup>b</sup>Dept. of Aerospace Engineering, University of Michigan, Ann Arbor, MI 48109, USA

## ARTICLE INFO

### Article history:

Received 8 January 2009

Received in revised form 24 March 2009

Accepted 6 April 2009

Available online 23 April 2009

### Keywords:

Entropy conservation

Entropy production

Entropy-stability

Entropy consistency

Shock stability

## ABSTRACT

In this paper, an entropy-consistent flux is developed, continuing from the work of the previous paper. To achieve entropy consistency, a second and third-order differential terms are added to the entropy-conservative flux. This new flux function is tested on several one dimensional problems and compared with the original Roe flux. The new flux function exactly preserves the stationary contact discontinuity and does not capture the unphysical rarefaction shock. For steady shock problems, the new flux predicts a slightly more diffused profile whereas for unsteady cases, the captured shock is very similar to those produced by the Roe- flux. The shock stability is also studied in one dimension. Unlike the original Roe flux, the new flux is completely stable which will provide as a candidate to combat multi-dimensional shock instability, particularly the carbuncle phenomenon.

© 2009 Elsevier Inc. All rights reserved.

## 1. Entropy consistency

Systems of conservation laws that originate in physics frequently possess an additional conservation law for an auxiliary quantity called entropy, which is conserved in smooth solutions but increases (or decreases according to the sign convention adopted) if shock waves appear. Numerical methods for conservation laws can be expected to reveal this behavior in a general way, but only for certain methods will the correspondence be precise. A method is said to be entropy-conservative if the local changes of entropy are exactly the same as predicted by the entropy conservation law. It is said to be entropy-stable if it produces more entropy than an entropy-conservative scheme.

In a previous paper [16], a new entropy-conservative scheme was proposed that is relatively inexpensive, and therefore a good candidate to be the foundation for controlling entropy production. This scheme also has the property of exactly preserving stationary contact discontinuities. An entropy-stable extension was also shown in [16], following [2]. The present paper is focused on guaranteeing that the amount of entropy produced is also correct (entropy-consistent) and to investigate the effects of entropy consistency on shock stability, which may be strongly connected to the carbuncle phenomenon [12].

### 1.1. Entropy conservation and entropy-stability

The physical conservation laws take the differential form in one dimension

$$\partial_t \mathbf{u} + \partial_x \mathbf{f} = 0 \quad (1a)$$

\* Corresponding author.

E-mail addresses: [aefarzad@eng.usm.my](mailto:aefarzad@eng.usm.my) (F. Ismail), [philroe@umich.edu](mailto:philroe@umich.edu) (P.L. Roe).

with the integral form

$$\oint (\mathbf{u} dx - \mathbf{f} dt) = 0 \tag{1b}$$

The additional conservation law has the differential form in one dimension

$$\partial_t U + \partial_x F \leq 0 \tag{2a}$$

with the integral form

$$\oint (U dx - F dt) \leq 0 \tag{2b}$$

Equality prevails in regions of smooth flow. Inequality may hold if the flow contains discontinuities. The sign is a matter of convention; for ideal gas dynamics these equations are correct if one takes  $U = -\rho g(s)$ ,  $F = -\rho u g(s)$  with

$$s = \ln p - \gamma \ln \rho$$

being the physical entropy. The sign convention is common in the mathematical and computational literature but creates some linguistic tension. Where inequality holds we will speak of entropy production which seems natural from a physical viewpoint, but we need to remember that  $U$  is being reduced.

The integral

$$\dot{U} = \int \int_{\Omega} (\partial_t U + \partial_x F) dx dt = \oint_{\partial\Omega} (U dx - F dt) \tag{3}$$

can be identified with the entropy production in a domain  $\Omega$  with boundary  $\partial\Omega$ . In all cases where entropy is produced, the physical mechanism responsible is on that is not represented in (1b). Typically it is a dissipative or dispersive process, represented mathematically by higher-order derivatives multiplied by some small parameter.

In a discrete version of the governing equations, it is usually accepted that the conservation laws (1b) must be observed, and some motivation to try and enforce equality in (2b) also, in smooth regions. The question then is how to enforce inequality in (2b) at discontinuities, not only with the proper sign (entropy-stable), but in the right amount. We now make some observations concerning the significance of the amount.

### 1.2. Entropy production and shock resolution

Consider a steady, one dimensional, discrete representation of a shockwave. Assume that this has been produced by some stable, consistent, conservative numerical method, with boundary conditions at inflow and at the outflow derived from the Rankine–Hugoniot jump conditions. Whether or not the scheme makes explicit reference to entropy, there will be some entropy flux  $\dot{m}S_i$  at the inflow (where  $\dot{m}$  is the mass flow rate) and some entropy flux  $\dot{m}S_o$  at outflow. The nature of the scheme guarantees that these are correct, because they can be derived from conserved variables, which are certainly correct.

The difference of the two entropy fluxes is accounted for by entropy production within the domain. It follows that entropy production within the domain is correct under the stated assumptions, once a steady state has been reached. Of course, if no entropy is produced, the scheme could not be stable.

However, entropy production during the transient phase of the calculation affects the quality of the shockwave that is eventually produced. This statement will now be illustrated in the case of a scalar conservation law,

$$\partial_t u + \partial_x f = \partial_t u + f'(u)\partial_x u = 0 \tag{4}$$

for which we choose an entropy function  $U(u) = u^2$ . To conform to the physicists view that entropy is naturally increasing with time, and brings disorder, we might define the “physical entropy” as  $S(u) = -u^2$ .

Consider a discrete shock representation  $u(x_j) = u_j^n$  ( $j = 1 \dots J$ ), that has not yet reached equilibrium, and suppose that during one time step, as it advances toward equilibrium, the solution changes to  $u(x_j) = u_j^{n+1}$ . Because of conservation, the mean value  $\bar{u}$  will not be changed. The “physical entropy” contained in the domain is (after dropping the superscripts)

$$\sum = - \sum_j (u_j)^2 \tag{5}$$

$$= - \sum_j (u_j - \bar{u} + \bar{u})^2 \tag{6}$$

$$= - \sum_j (u_j - \bar{u})^2 - 2\bar{u} \sum_j (u_j - \bar{u}) - J\bar{u}^2 \tag{7}$$

$$= - \sum_j (u_j - \bar{u})^2 - J\bar{u}^2 \tag{8}$$

It is clear that any change that moves  $u_j$  closer to  $\bar{u}$  increases the entropy, and also smears the shockwave. Conversely, moving  $u_j$  away from  $\bar{u}$  reduces the entropy, but if  $u_j$  is moved too far away from  $\bar{u}$ , then overshoots are created.

It becomes apparent that entropy enters into shock quality in two-ways. First, the rise of entropy across the shock must be correct. However, this is rather easy, merely requiring conservation and stability. But secondly, the entropy contained within the shock should be neither too great nor too small, otherwise the shock will respectively be smeared out, or oscillatory. The “correctness” of this quantity in the steady state depends on its generation during the transient phase.

However, it does not seem easy to make a direct analytical connection between entropy production and shock quality, and so much of the present paper rests on numerical experiment. However, all we seek is a “reasonable” shock profile, since it seems quite hard to define an optimal one.

## 2. Entropy production in scalar problems

### 2.0.1. Analytical behavior

We continue the discussion of the scalar conservation law (4) with its entropy function  $U = -u^2$  and introduce also the entropy variable  $v(u) = dU/du = -2u$ , so that

$$\partial_t U + f'(u)\partial_x U = \partial_t U + \partial_x F = 0 \quad (9)$$

where

$$F = \int_{u_0}^u v(u) \frac{df}{du} du$$

It is well known that the “conservation law” (9) breaks down as soon as discontinuities develop. For example, if we draw a control volume around a small section of a shock, we can find the rate of entropy production within that volume by integrating

$$\oint \partial \Omega (U dx - F dt) \quad (10)$$

which turns out to be of the order of the cube of the shock strength [8].

### 2.0.2. Discrete behavior

**Entropy conservation.** Following [16], consider two neighboring discrete states  $(u_{L,R})$  with dual cell area  $(h_{L,R})$ , discretized semi-discretely as

$$\begin{aligned} h_L \partial_t u_L &= f_L - f^* \\ h_R \partial_t u_R &= f^* - f_R \end{aligned} \quad (11)$$

and has two kind of interpretations. One, the left and right states are point values at vertices that surround a linear element centered at  $*$ . This is a residual distribution scheme where the residual  $(f_L - f_R)$  is split as  $(f_L - f^*) + (f^* - f_R)$  and distributed to the left and right states respectively. The other is finite volume interpretation where the left and right states are cell-averaged values separated by a flux interface  $*$ . An entropy update will be

$$\begin{aligned} h_L \partial_t U_L &= v_L (f_L - f^*) \\ h_R \partial_t U_R &= v_R (f^* - f_R) \end{aligned} \quad (12)$$

with the total element update computed as the sum of the two nodes given by

$$\partial_t (h_L U_L + h_R U_R) = -[vf] + [v]f^* \quad (13)$$

where  $[ \cdot ] = (\cdot)_R - (\cdot)_L$ . Define an entropy production  $\dot{U}$  associated with flux  $f^*$  be the difference of the entropy produced by that flux and the entropy produced by the discrete entropy conserving equation (Eq. (3)). In a finite volume scheme with numerical flux  $f^*(u_L, u_R)$ , the entropy production at each interface is

$$\dot{U} = f^*(u_L, u_R)(v_R - v_L) - (v_R f_R - v_L f_L) + (F_R - F_L) \quad (14)$$

and choosing  $f^*$  to make this expression vanish will result in an entropy-conservative scheme.

If instead, we choose the arithmetic mean flux  $f^* = \frac{1}{2}(f_L + f_R)$ , then we obtain

$$\dot{U} = (F_R - F_L) - \frac{1}{2}(v_R + v_L)(f_R - f_L) \quad (15)$$

$$= \int_0^1 (v - \bar{v}) \frac{df}{du} [u] d\xi \quad (16)$$

$$= [u] \int_0^1 (\xi - \frac{1}{2}) [v] \frac{df}{du} d\xi \quad (17)$$

$$= O[u]^3 \quad (18)$$

In smooth regions this production is below the truncation error of the central difference scheme, but in non-smooth regions it is large and of unpredictable sign. We therefore replace the arithmetic mean flux by an entropy-conservative flux<sup>1</sup>. For Burgers' equation with  $f = \frac{1}{2}u^2$ , this is

$$f_c^* = \frac{1}{6}(u_L^2 + u_L u_R + u_R^2) \tag{19}$$

Note that this is a symmetric function of the left and right states, and hence involves no upwinding.

**Upwinding.** To give stability to the discretization, one adds an upwind term so that the flux reads

$$f^* = f_c^* - \frac{1}{2}|\bar{a}||u| \tag{20}$$

or, better from a theoretical point of view for extension to systems,

$$f^* = f_c^* - \frac{1}{2}|\bar{a}|\frac{du}{dv}[v] \tag{21}$$

so that

$$\dot{U} = -\frac{1}{2}|\bar{a}|\frac{du}{dv}[v]^2 \tag{22}$$

and the entropy due to upwinding has the proper sign. Note that  $\bar{a} = \frac{a_L + a_R}{2}$  is the averaged velocity at the interface \*. For Burgers' equation, the extra term is

$$F_U^* = -\frac{1}{2}|u_L + u_R|(u_R - u_L)$$

leading to the *entropy-stable* flux

$$f_S^* = \frac{1}{6}(u_L^2 + u_L u_R + u_R^2) - \frac{1}{4}|u_L + u_R|(u_R - u_L) \tag{23}$$

**Production.** The entropy due to upwinding is not, however, large enough. It was noted above that the entropy produced by shock waves is of the order of the cube of the shock strength. This suggests that the numerical flux should also contain a term proportional to the square of the disturbance, because this would contribute a term of the order  $[u]^3$  to  $\dot{U}$ . The arithmetic mean flux does add a term of the proper order of magnitude at shocks, but subtracts it at rarefactions. Our expectation was that a third-order term should only be added if a shock has been detected.

In fact, our numerical experiments did not quite bear this out. We ended up by adding a term proportional to  $||u|||u|$  to the flux, and hence a term proportional to  $||u|||u|^2$  (and so of the correct sign) to  $\dot{U}$ , in all circumstances. For weak disturbances, including well-resolved rarefaction waves, the extra effect is small. For shocks, the extra dissipation removes oscillations, and for under-resolved rarefactions, it provides a smoothing that was found empirically to improve results.

The final form of our recommendation is

$$f^* = f_c^* - \frac{1}{2}(|\bar{a}| + \alpha|a|)\frac{du}{dv}[v] \tag{24}$$

Making the third term proportional to the jump in wavespeed gives the correct order of magnitude for nonlinear flux functions, but gives no contribution for linear flux functions. At this stage,  $\alpha$  is a parameter to be determined, and this is the topic of the next section.

### 3. A theoretical attempt at consistency

Entropy consistency, in this sense of 'just enough', seems to be difficult to analyze. This is because we can expect that shocks will be captured over several cells, and the total entropy required will have to be generated at more than one interface. Unlike entropy conservation, the problem will no longer be local. Some analysis can be done by assuming that it is local, but this may not be completely satisfactory. It is given below for the simple case of Burgers equation.

#### 3.1. Scalar equations

Consider a rectangular control volume in the  $x, t$  plane whose dimensions are  $Dx, Dt$  (see Fig. 1). Let this control volume be traversed by a shock, possibly of finite thickness, moving with speed  $\lambda$ , with uniform states on either side of it. Compute

$$I = \oint (U dx - F dt) \tag{25}$$

<sup>1</sup> We intend, of course, to reintroduce a suitable production term later on.

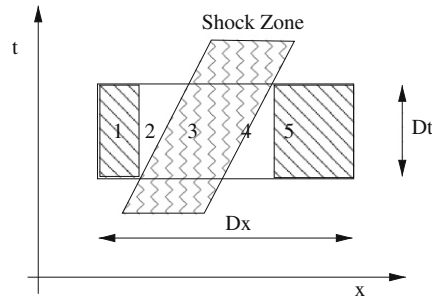


Fig. 1. Control volume to establish source term in entropy conservation law.

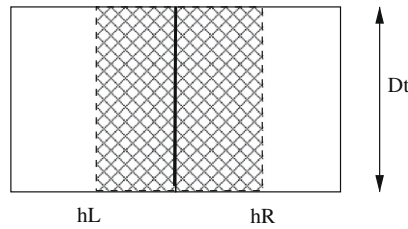


Fig. 2. Control volume to establish entropy production at an interface.

Regions 1, 3 and 5 do not contribute to  $I$ . The contribution from regions 2 and 4 are easily found; we have

$$I = \lambda \Delta t [U] - [F] \Delta t \tag{26}$$

Next evaluate  $I$  for the control volume shown in Fig. 2 drawn around a typical cell interface. Then

$$I = ([vf] - [v]f^* - [F]) \Delta t \tag{27}$$

Equating the two expressions for  $I$  (asking this interface to produce all of the entropy for the shock ) gives

$$[v]f^* = [vf] - \lambda [U] \tag{28}$$

The difference between this equation and the one derived from entropy conservation (2b) is the appearance on the right of  $\lambda[U]$  rather than  $[F]$ .

This indicates that we should add to the flux a production term  $f_p^*$  satisfying

$$[v]f_p^* = [F] - \lambda [U] \tag{29}$$

For Burgers equation, with the choice of entropy variable adopted in Section 2.0.1, this additional flux is  $\frac{1}{12}[u]^2$ ; it amounts to taking  $\alpha = \frac{1}{6}$  in (24). For fluxes between very different states it will be significant, and should be added to the entropy-stable flux if shocks are detected. The resulting flux turns out to be [5]

$$f^* = \frac{1}{4}(u_L^2 + u_R^2) - \frac{1}{2} \frac{|u_L + u_R|}{2} (u_R - u_L) \tag{30}$$

This is simply the arithmetic mean flux with a standard upwind flux<sup>2</sup>. However, as mentioned in Section 2.0.2, we add the production term for all circumstances (includes both compression and expansion cases) to obtain the *entropy-consistent* flux;

$$f^* = \frac{1}{6}(u_L^2 + u_L u_R + u_R^2) - \frac{1}{4}|u_L + u_R|(u_R - u_L) - \frac{|u_R - u_L|(u_R - u_L)}{12} \tag{31}$$

The first term is entropy conserving. The second (upwind) term enforces entropy-stability, and the third term yields entropy production of  $O([u]^3)$ . Recall that the exact Riemann solver for the Burgers equation is

$$f^* = \begin{cases} 0 & \text{if } u_L < 0 < u_R \\ \frac{u_L^2}{2} & \text{else if } u_L + u_R \geq 0 \\ \frac{u_R^2}{2} & \text{else } u_L + u_R < 0 \end{cases} \tag{32}$$

<sup>2</sup> In other words Roe's approximate Riemann solver with no "entropy fix".

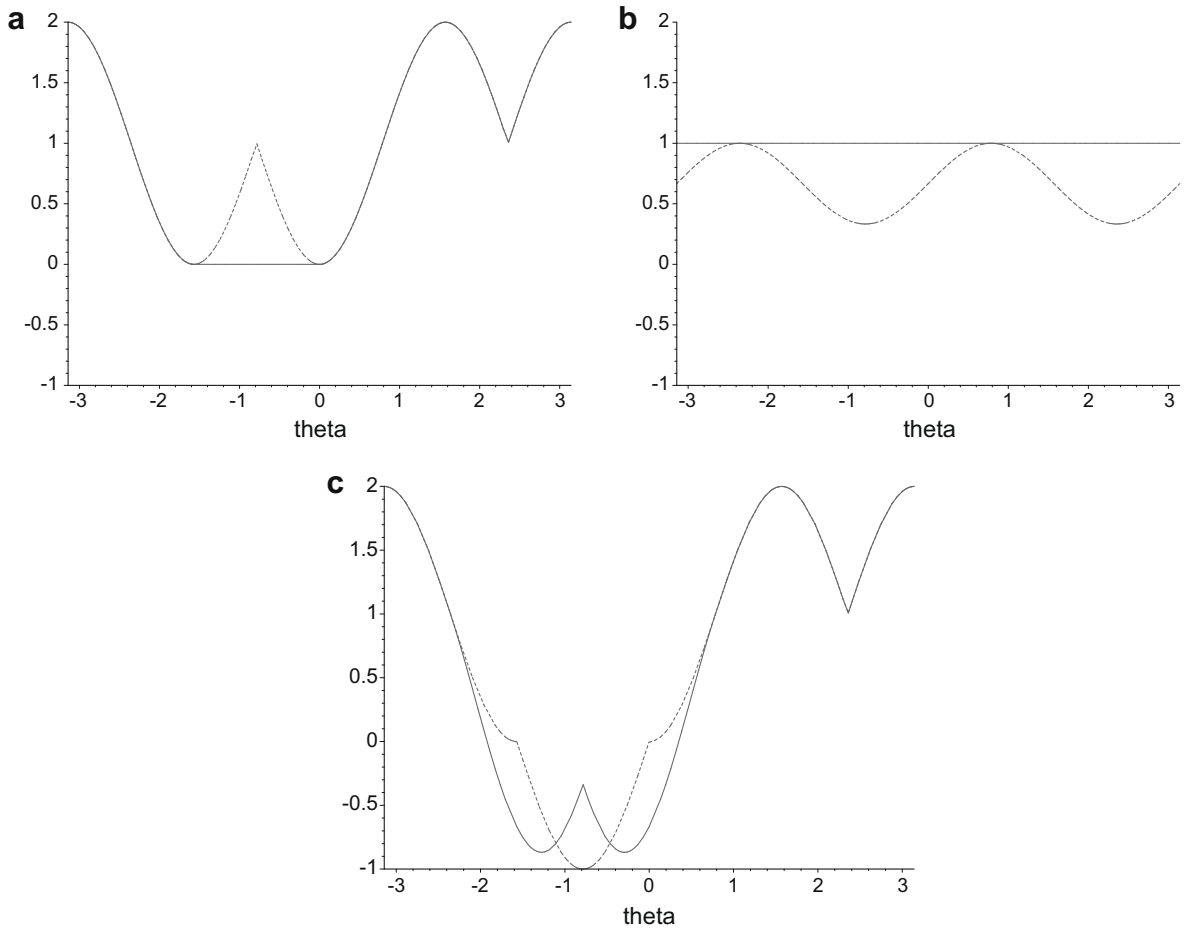


**Fig. 3.** (a) Dimensionless comparison of the Godunov flux (solid line) with the Roe flux (dotted); (b) dimensionless comparison of the arithmetic mean flux (solid line) with the entropy conserving flux (dotted); (c) dimensionless comparison of the entropy consistent flux (solid line) with [15] entropy fixed flux (dotted).

To make a graphical comparison between the various flux formulae, we may nondimensionalize them with respect to the arithmetic mean flux as

$$\mathcal{F}^* = \frac{4f^*}{(u_L^2 + u_R^2)} \tag{33}$$

To display this, Fig. 3 plots  $\mathcal{F}^*(\sin \theta, \cos \theta)$  versus the parameter  $\theta$  with  $-\pi \leq \theta \leq \pi$ .

For the Burgers equation, the only difference between the exact Riemann solver and the flux is in the two-way rarefaction region ( $u_L \leq 0 \leq u_R$ ). The former sees the interface flux always as zero in rarefactions, but the latter does not. Fig. 3(b) compares two nonupwinded fluxes (arithmetic mean and entropy conserving). Fig. 3(c) displays the entropy consistent flux Eq. (31), which is negative in the two-way rarefaction region. This is surprising at first, but it may be recalled that the dissipation in the “exact” flux formula is in fact the minimum required to avoid rarefaction shocks. To give smooth rarefactions a greater dissipation, a negative flux is needed [10,15]. The proposal made in [15] was simply  $f^* = \frac{1}{2} u_L u_R$ , which is also plotted.

In the next section, numerical experiments will be conducted to try and validate this analysis.

#### 4. Experiments on Burgers equation

Only a small selection of the experiments that we carried out are reported here, and they are edited to tell a story. For each experiment, we prescribed 40 cells with periodic boundary conditions. The Courant number is 0.8 and the solid lines represent the exact solutions and are compared against the results of the new schemes (ES (entropy-stable or  $\alpha = 0.0$ ) and EC (entropy-consistent or  $\alpha = 1/6$ ) fluxes). The computations are done using a first order spatial and temporal accurate method unless stated otherwise.

4.1. Test case I: modelling rarefaction with a stationary shock

The first test problem is an initial value problem [7] with data

$$u(x, 0) = \begin{cases} -1 & \text{if } \frac{1}{3} \leq |x| \leq 1 \\ 1 & \text{if } |x| < \frac{1}{3} \end{cases} \tag{34}$$

and computed until  $t = 0.32$ . This initial square wave will evolve into a rarefaction fan on the left while the right side will remain a stationary shock. Note that this problem will contain a sonic point rarefaction. The exact solution to this problem is given in [7]. For this example, in the rarefaction zone ( $u_L < 0 < u_R$ ) where initially  $|u_L| = |u_R|$ , the net change for Roe flux is  $[f] = 0$ , so we expect the unphysical rarefaction shock is unchanged. For the exact Riemann solver where  $u_{i-1} = -1.0, u_i = -1.0, u_{i+1} = 1.0, [f] = -\frac{u_i^2}{2}$ , so  $u_i$  will increase by this amount (multiplied by  $-v$ ) hence breaking up the rarefaction shock. For the ES solver,  $[f] = -\frac{u_i^2}{3}$ , again we expect  $u_i$  to increase avoiding rarefaction shock. For the EC solver,  $[f] = -\frac{2u_i^2}{3}$  which increases  $u_i$  slightly more than the exact Riemann solver. The net flux change for ES/EC flux only differs by a factor of  $\frac{1}{6}$  compared to the exact Riemann solver. Initially, the rarefaction regions produced by the ES/EC flux and exact Riemann solver are slightly different but as time evolves, the rarefactions should be similar since their profiles become relatively smooth. Of course, the Roe flux and the exact Riemann solver should preserve the stationary shock ( $x = \frac{1}{3}$ ) and we predict that the new flux (at least EC) to do the same.

Our numerical results confirmed that the new flux functions (ES and EC) do not see the rarefaction as a rarefaction shock (Figs. 5–7) unlike the original Roe flux where its solution is identical to the initial condition (Roe flux solution is omitted for brevity). This is one of the benefits of including a more precise control of entropy. In fact, the new flux functions produce rarefactions that are comparable to the exact Riemann solver solution (Fig. 4) as predicted before.

Unfortunately, Fig. 5 clearly demonstrates spurious oscillations being produced near the shock by the ES flux, since there is not enough entropy being generated across the shock. In other words, the solution is not monotone even for a first order method. Adding the entropy consistency term removes these spurious oscillations (Fig. 6) and provides extra smoothing for the under-resolved rarefaction. Using a second order TVD version (harmonic limiter) based on Hancock scheme adds further improvement to the prediction of the rarefaction (Fig. 7).

4.2. Test case II: modelling compression waves

Consider the following initial value problem.

$$u(x, 0) = \begin{cases} u_0 & \text{if } |x| > 1 \\ u_0 - u_1 * \sin \pi x & \text{if } -1 \leq x \leq 1 \end{cases} \tag{35}$$

where the amplitude  $u_1 = 0.5$  has been chosen. The background velocity  $u_0$  is chosen to be 0.0 (although in [5], we also have used  $u_0 = 1.0, 5.0$  and produced similar results.). This is an initial value problem which also consists of compression and expansion waves. However, the normalized analytical solution will be in the form of

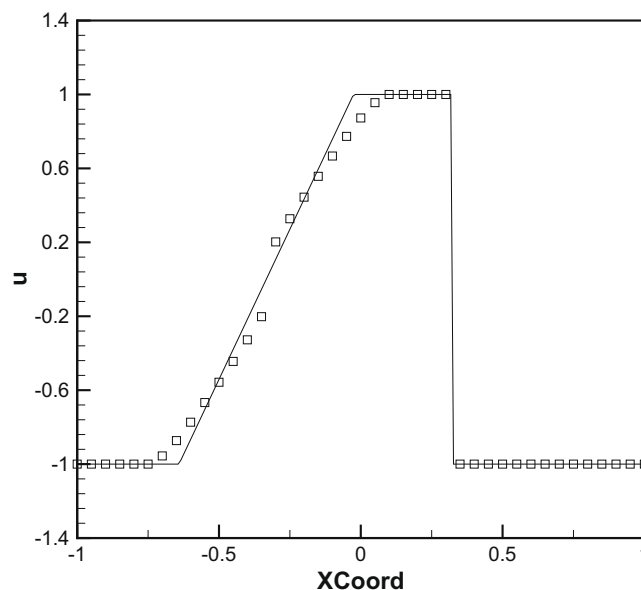


Fig. 4. Test 1 – Exact Riemann solver.

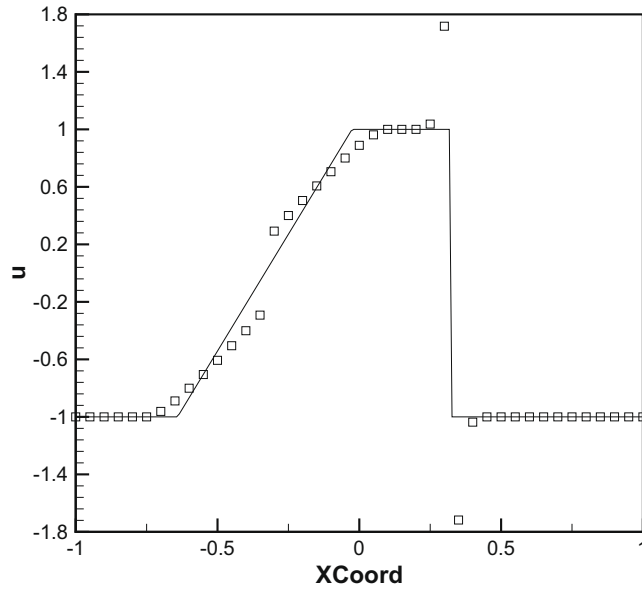


Fig. 5. Test 1 – ES flux. Overshoots are due to not enough entropy being produced.

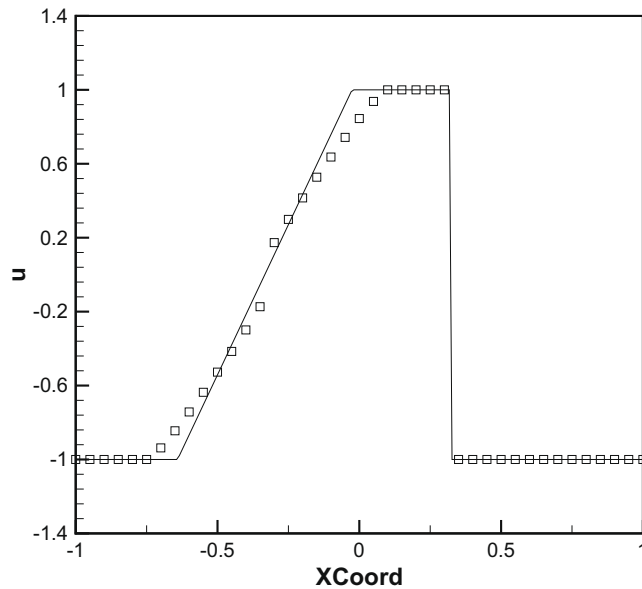


Fig. 6. Test 1 – EC flux. With a proper entropy production we have a monotone solution.

$$u(x, t) = \frac{u_0}{u_1} - \sin\left(\pi x - \frac{u}{u_1} u_1 t\right) \tag{36}$$

Figs. 8–11 indicate that for smooth data, the solutions are almost identical regardless if we add the  $\frac{1}{12}[u]^2$  term or not. This is consistent with our theoretical prediction where entropy production for the EC flux is of  $O([u]^3)$  as opposed to  $O([u]^2)$  for the ES flux. However, for data with high gradients (as in test case 1), the two fluxes produced results that are substantially different. This reinforces the importance of producing the correct amount of entropy.

## 5. Systems of Euler equations

### 5.1. The form of the flux

The Euler equations for an ideal gas in one dimension are

$$\partial_t \mathbf{u} + \partial_x \mathbf{f} = \partial_t \mathbf{u} + \mathbf{A} \partial_x \mathbf{u} = 0 \tag{37}$$

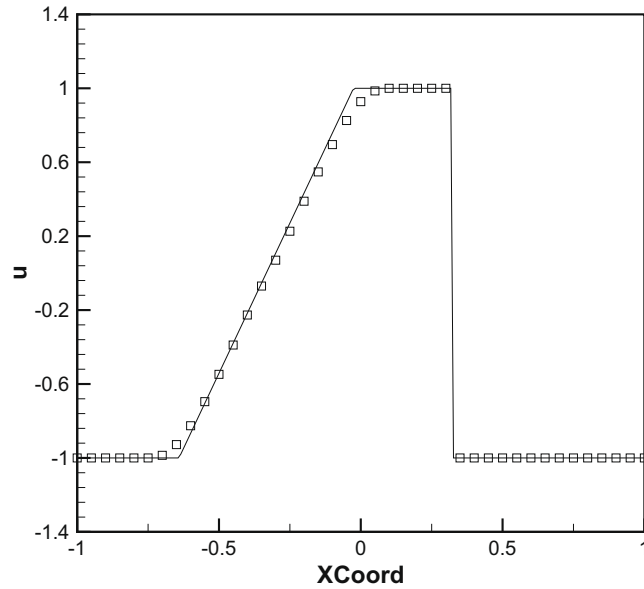


Fig. 7. Test 1 – Second order EC flux.

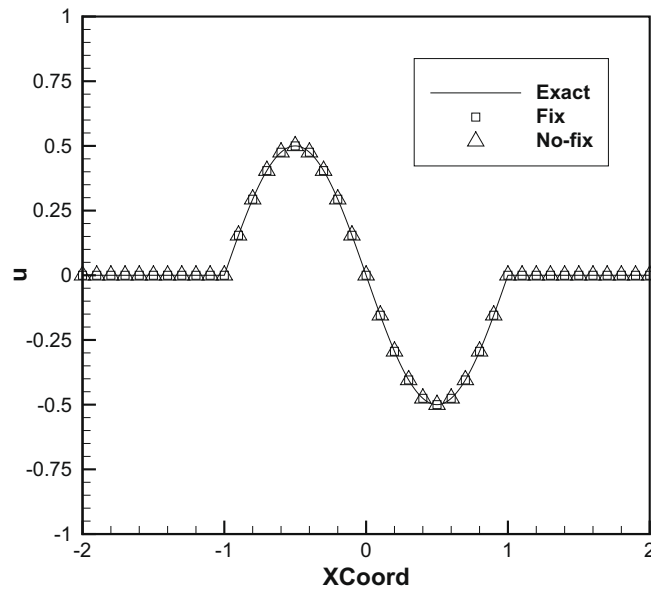


Fig. 8. Test 2 –  $t = 0$ . Note squares denote EC flux whereas triangles denote ES flux.

where

$$\mathbf{u} = (\rho, \rho u, \rho E)^T \tag{38}$$

$$\mathbf{f}(\mathbf{u}) = (\rho u, \rho u^2 + p, \rho u H)^T \tag{39}$$

The total energy is defined as  $E = e + \frac{u^2}{2}$  and the total enthalpy  $H = E + \frac{p}{\rho}$ . The pressure is determined from the equation of state,  $e = \frac{p(\gamma-1)}{\rho}$  where  $\gamma$  is the ideal gas constant and  $\mathbf{A}$  is the Jacobian matrix. Define the entropy function<sup>3</sup> to be  $U = -\frac{\rho s}{\gamma-1}$  where  $s = \ln p - \gamma \ln \rho$  is the physical entropy, we compute the entropy variables as

$$\mathbf{v} = \frac{\partial U}{\partial \mathbf{u}} = \left( \frac{\gamma - s}{\gamma - 1} - \frac{1}{2} \frac{\rho}{p} (u^2), \frac{\rho u}{p}, -\frac{\rho}{p} \right)^T \tag{40}$$

<sup>3</sup> This is the only choice of entropy function that generates entropy variables  $\mathbf{v}$  that can be extended to the Navier–Stokes equations [4].

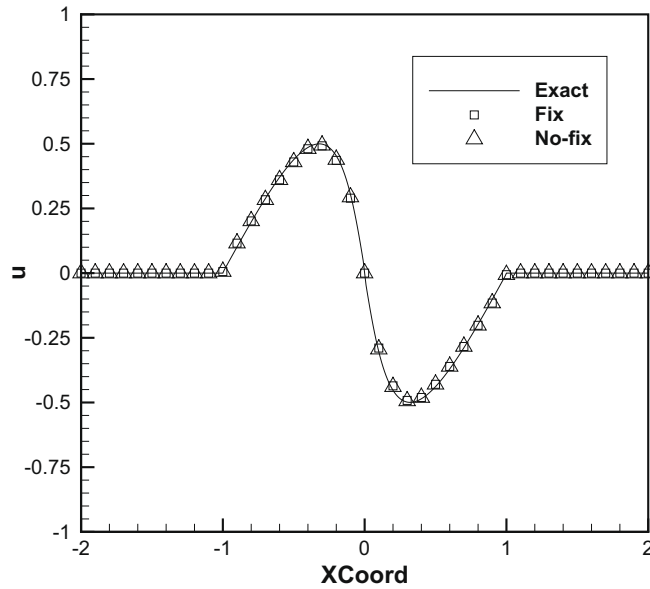


Fig. 9. Test 2 – Solution at  $t = 0.32$ . Both fluxes demonstrate almost identical results for smooth data.

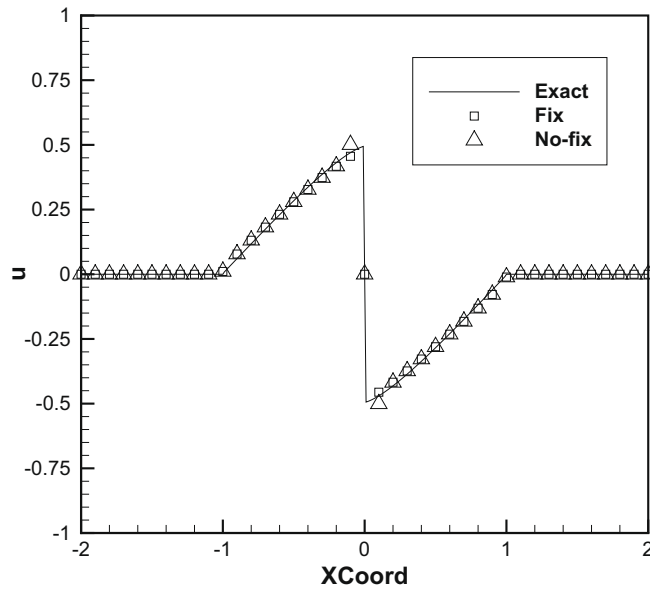


Fig. 10. Test 2 – Solution at  $t = 0.96$ . As compression waves begins to steepen up, the fluxes starts to slowly differ from each other at the compression region.

An entropy-stable flux [2,16] for the Euler equations is

$$\mathbf{f}^* = \mathbf{f}_c - \frac{1}{2} \hat{\mathbf{R}} \hat{\mathbf{D}} \hat{\mathbf{R}}^T [\mathbf{v}] \tag{41}$$

where  $\mathbf{f}_c$  is the entropy-conservative flux [16] (included in Appendix A) and  $\hat{\mathbf{R}}$  contains the averaged right eigenvectors of  $\mathbf{A}$

$$\hat{\mathbf{R}} = \begin{bmatrix} 1 & 1 & 1 \\ \hat{u} - \hat{a} & \hat{u} & \hat{u} + \hat{a} \\ \hat{H} - \hat{u}\hat{a} & \frac{1}{2}\hat{u}^2 & \hat{H} + \hat{u}\hat{a} \end{bmatrix} \tag{42}$$

and  $\hat{\mathbf{D}}$  is a positive dissipation matrix that is written as

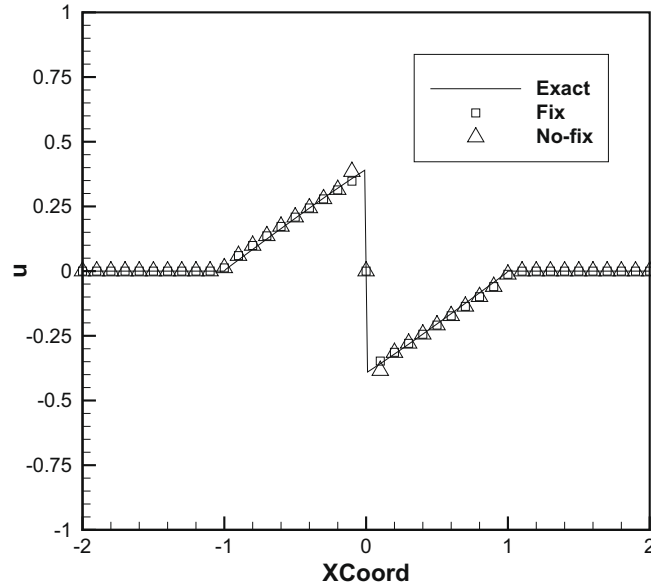


Fig. 11. Test 2 – Solution at  $t = 1.44$ . As the shock develops, it is clear that only the EC flux is monotone.

$$\hat{\mathbf{D}} = \hat{\Lambda} \hat{\mathbf{S}} \tag{43}$$

where  $\hat{\Lambda}$  is the matrix of absolute eigenvalues

$$\hat{\Lambda} = \text{diag}(|\hat{u} - \hat{a}|, |\hat{u}|, |\hat{u} + \hat{a}|) \tag{44}$$

and  $\hat{\mathbf{S}}$  is a matrix that produces the correct scaling

$$\hat{\mathbf{S}} = \text{diag}\left(\frac{\hat{\rho}}{2\gamma}, \frac{(\gamma - 1)\hat{\rho}}{\gamma}, \frac{\hat{\rho}}{2\gamma}\right) \tag{45}$$

such that  $\mathbf{R}^{-1} d\mathbf{u} = \mathbf{S}\mathbf{R}^T d\mathbf{v}$ . The averaged ( $\hat{\cdot}$ ) values for the asymmetric flux ( $\hat{\mathbf{R}}\hat{\mathbf{D}}\hat{\mathbf{R}}^T[\mathbf{v}]$ ) are determined exactly as the averaged values for  $\mathbf{f}_c$  [5]. These averaged quantities, particularly for density and speed of sound ensure that stationary contact discontinuities are preserved [16] while for other variables are for the sake of computational economy.

If we form the integral (25) for a system of conservation laws, the control volume may be crossed by several  $k$  waves. If these waves do not intersect, then we will have

$$I = \Delta t \left( \sum_k \lambda_k [U]_k - [F] \right) = \Delta t \sum_k (\lambda_k [U]_k - [F]_k) \tag{46}$$

We will assume that the same formula is true if they do intersect. Contact and rarefactions waves do not contribute to (46), so the summation is simply over any shockwaves that may be present. If we introduce a flux component  $\mathbf{f}_p$  to cater for production, then we easily find that

$$[\mathbf{v}]^T \mathbf{f}_p = \sum_{shocks} ([F] - \lambda[U]) \tag{47}$$

and we now turn to evaluating the quantity  $([F] - \lambda[U])$  for a single shock.

In manipulating this expression, we will use results from Roe-linearization [14], since these are exact whenever the only wave present is a shock. We employ the Roe-averaging  $\tilde{q}$  defined by

$$\tilde{q} = \frac{\sqrt{\rho_L} q_L + \sqrt{\rho_R} q_R}{\sqrt{\rho_L} + \sqrt{\rho_R}} \tag{48}$$

and the complementary averaging

$$\tilde{\tilde{q}} = \frac{\sqrt{\rho_L} q_R + \sqrt{\rho_R} q_L}{\sqrt{\rho_L} + \sqrt{\rho_R}} \tag{49}$$

noting the identity

$$[ab] = \tilde{a}[b] + \tilde{\tilde{b}}[a] \tag{50}$$

We have, across an isolated shock,

$$[F] - \lambda[U] = [uU] - (\tilde{u} \pm \tilde{a})[U] = \tilde{u}[U] + \tilde{U}[u] - \tilde{u}[U] \mp \tilde{a}[U] = \tilde{U}[u] \mp \tilde{a}[U]$$

where the upper (lower) sign relates to right (left)- going waves.

Recall that  $U = -\rho S / (\gamma - 1)$  [16], we easily find that

$$\tilde{U} = \frac{-1}{\gamma - 1} \tilde{\rho} \tilde{S}, \quad [U] = \frac{-1}{\gamma - 1} (\tilde{\rho}[S] + \tilde{S}[\rho])$$

where  $\tilde{\rho} = \sqrt{\rho_L \rho_R}$  so that

$$[F] - \lambda[U] = \frac{-1}{\gamma - 1} (\tilde{\rho} \tilde{S}[u] \mp \tilde{a}(\tilde{\rho}[S] + \tilde{S}[\rho]))$$

Now, the acoustic eigenvector in the Roe-averaging is  $[1, \tilde{u} \pm \tilde{a}, \tilde{H} \pm \tilde{u}\tilde{a}]^T$  and hence

$$[\rho u] = \tilde{\rho}[u] + \tilde{u}[\rho] = (\tilde{u} \pm \tilde{a})[\rho] \Rightarrow \tilde{\rho}[u] = \pm \tilde{a}[\rho]$$

thus we finally have,

$$[F] - \lambda[U] = \frac{\pm \tilde{\rho} \tilde{a}}{\gamma - 1} [S]$$

which is an exact result.

From now on, however, we make weak shock assumptions. A combination of standard results [1] yields

$$[S] \approx \frac{\gamma^2 - 1}{12\gamma} \left( \frac{[\rho]}{\rho} \right)^3 \tag{51}$$

so that

$$[F] - \lambda[U] \approx \frac{\gamma + 1}{12\gamma} \rho a \left( \frac{[\rho]}{\rho} \right)^3 \tag{52}$$

Let us compare this with the entropy produced by the proposed flux, again for an isolated shock (of either family). The formula to be evaluated is

$$\dot{U} = \frac{\alpha}{2} [\mathbf{v}]^T \mathbf{R} |[\Lambda S]| \mathbf{R}^T [\mathbf{v}] \tag{53}$$

$$= \frac{\alpha}{2} \left( \frac{2[\rho]}{\rho} \right)^2 \left( \frac{\rho}{2\gamma} \right) \left( \frac{\gamma + 1}{2} a \frac{[\rho]}{\rho} \right) \tag{54}$$

$$= \frac{\alpha}{2} \frac{\gamma + 1}{\gamma} \rho a \left( \frac{[\rho]}{\rho} \right)^3 \tag{55}$$

and this matches the required result if  $\alpha = \frac{1}{6}$ , exactly as for Burgers equation.

Therefore, we propose an *entropy-consistent* flux function using Eq. (41) with the following dissipative matrix

$$\hat{\mathbf{D}}_{EC1} = \left( \hat{\Lambda} + \frac{1}{6} |[\Lambda_{u \pm a}]| \right) \hat{\mathbf{S}} \tag{56}$$

where  $[\Lambda_{u \pm a}] = \text{diag}([u - a], 0, [u + a])$  adding extra dissipation only to the acoustic waves and hence entropy produced at  $O([\cdot]^3)$ . This will be referred to as EC1 flux in this paper.

## 6. Experiments on the Euler equations

### 6.1. Test case III: modelling a stationary shock

This is a one dimensional problem [3] with an interface separated by a left and right states with  $M_0$  being the upstream Mach number and  $\gamma = 1.4$ . The normalized upstream (state 0) and downstream (state 1) conditions are given by the Rankine–Hugoniot conditions

$$\begin{aligned} \mathbf{U}_0 &= \left[ 1 \quad 1 \quad \frac{1}{\gamma(\gamma-1)M_0^2} + \frac{1}{2} \right] \\ \mathbf{U}_1 &= \left[ f(M_0) \quad 1 \quad \frac{g(M_0)}{\gamma(\gamma-1)M_0^2} + \frac{1}{2f(M_0)} \right] \end{aligned} \tag{57}$$

where  $f(M_0)$  and  $g(M_0)$  are the jump conditions of density and pressure across the shock given by

$$f(M_0) = \left( \frac{2}{(\gamma + 1)M_0^2} + \frac{\gamma - 1}{\gamma + 1} \right)^{-1} \quad (58)$$

$$g(M_0) = \frac{2\gamma M_0^2}{(\gamma + 1)} - \frac{\gamma - 1}{\gamma + 1}$$

$\nu = 0.2$  is selected to avoid possible numerical instability issues associated with semi-discrete flux functions, although the new flux function seems to be stable for higher Courant numbers as proven in the unsteady case in Section 6.4. There are 25 computational cells and the initial supersonic conditions are applied at the inlet boundaries. At the subsonic outlet, zero gradients are prescribed for the fluxes except for the mass flux, where it is fixed to be unity. The reason for doing this is discussed when shock instability is investigated (Section 6.5).

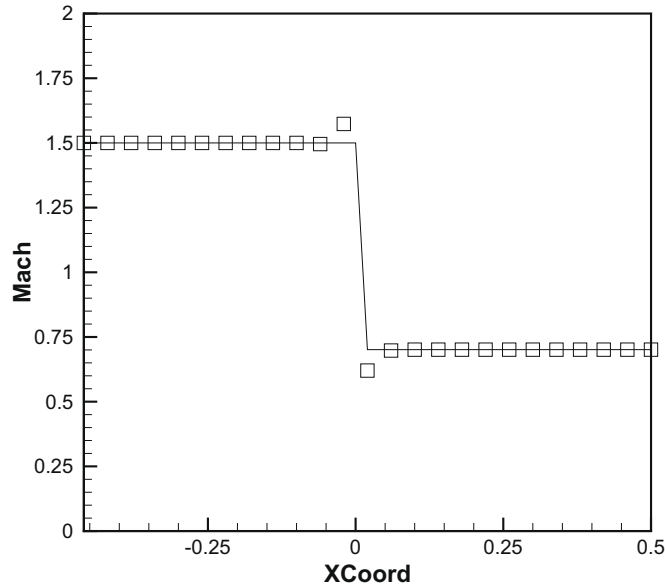


Fig. 12. Test 3 – ES flux with  $M_0 = 1.5$  with spurious over/undershoots near the shock.

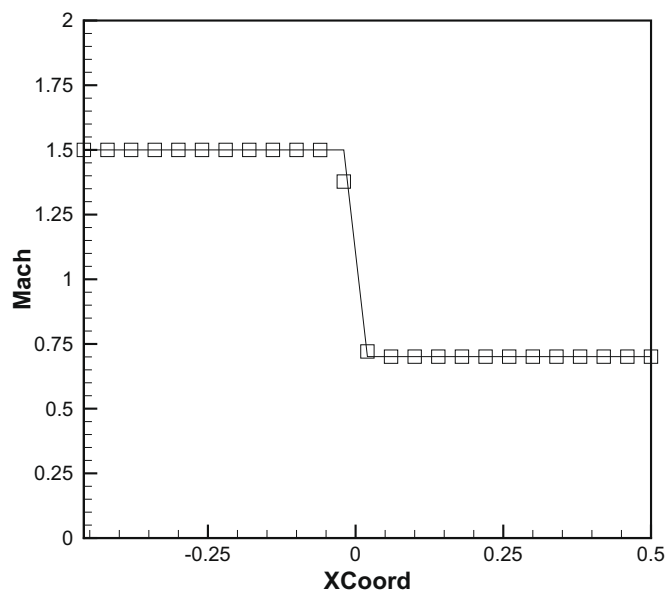


Fig. 13. Test 3 – EC1 flux with  $M_0 = 1.5$ . No over/undershoots.

The entropy-stable (ES) flux ( $\alpha = 0.0$ ) which has entropy produced only from the upwinding term does not show monotone shock profiles unlike (for most cases) the entropy-consistent (EC1) flux (Figs. 12–16). In addition, both ES and EC1 flux functions introduce multiple intermediate states (or cells) within the shock hence slightly smearing its profile. For the EC1 flux, the amount of smearing is directly proportional to the magnitude of  $\alpha$ . Reducing the current  $\alpha = 1/6$  steepens the shock but with the risk of generating spurious overshoots. On the other hand, selecting  $\alpha > 1/6$  increases the amount of entropy production (dissipation) at the shock.

Unfortunately for high  $M_0$ , the density profiles predicted by the EC1 flux show undershoots (refer to Fig. 17), which can be explained by the following. Our analysis is based on a local entropy production across shocks, captured by only one interface without intermediate cells. This assumption is perhaps reasonable for solving the Burgers equation but may not be accurate for solving the Euler equations since the shocks are captured over multiple intermediate cells with the number of interme-

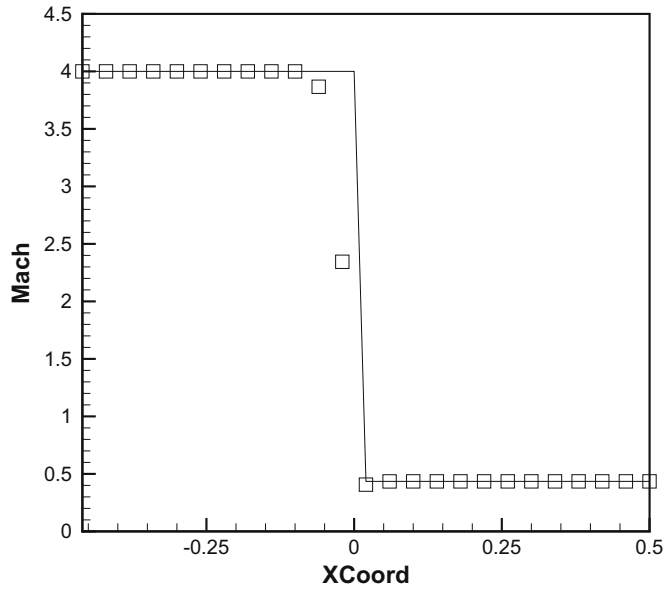


Fig. 14. Test 3 – ES flux with  $M_0 = 4.0$ . Not a monotone solution.

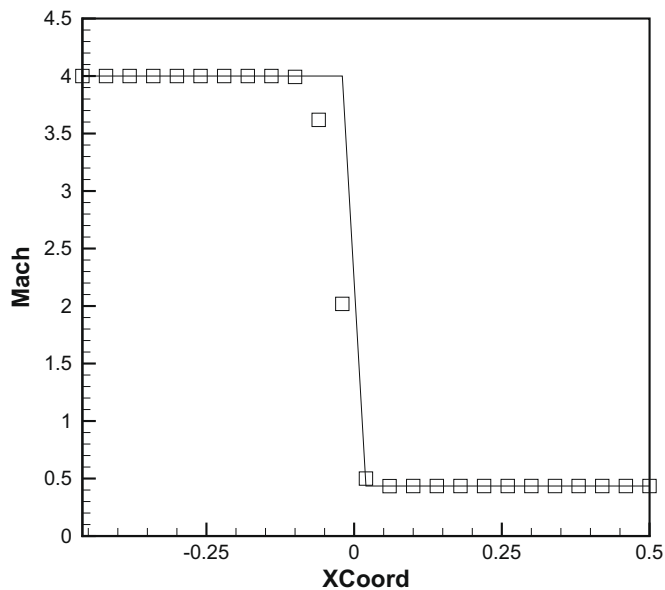


Fig. 15. Test 3 – EC1 flux with  $M_0 = 4.0$ . Monotone shock solution.

diated cells increases with increasing  $M_0$ . For example, assume entropy is produced at  $\alpha c[\rho]^3$  ( $c$  is a constant coefficient) for a particular shock with no intermediate cell. If one intermediate cell is introduced halfway within the shock, the total entropy production would still be the same but divided over two interfaces each with  $4\alpha c[\rho/2]^3$ . If we have more intermediate cells, we expect  $\alpha = 1/6$  to be multiplied with a larger value. Based on numerical experiments, the entropy-consistent flux produces shocks with three to four intermediate cells, hence  $\alpha$  must be a value between 1.5 and 2.6 to ensure enough entropy production.

Our numerical experiments indicate that the difference of the intermediate states is generally much larger (hence the term  $O([\rho]^3)$  is even larger) in the supersonic region of the shock compared to the subsonic region. As such, it may cause the solution to blow-up in the supersonic region if  $\alpha > 1.0$  is used since numerical diffusion becomes overwhelmingly dominant restricting the time-step stability. To overcome this shortcoming and produce 'enough' entropy in both the supersonic and subsonic regions in the shock, the following dissipative matrix is proposed:

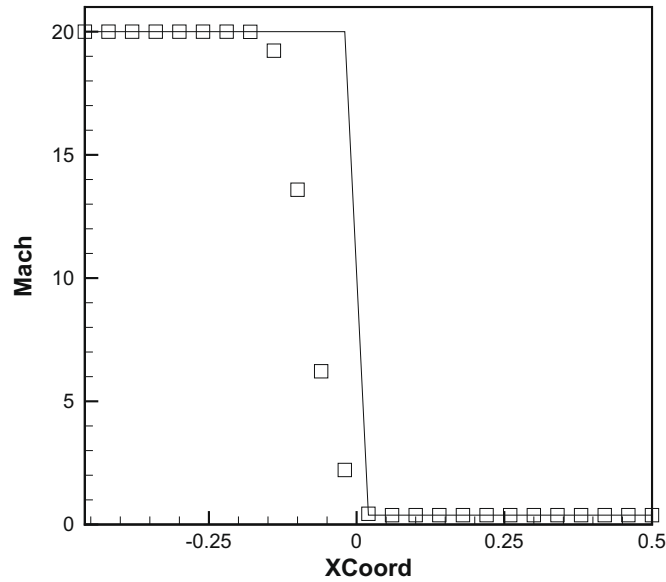


Fig. 16. Test 3 – EC1 flux with  $M_0 = 20.0$ .

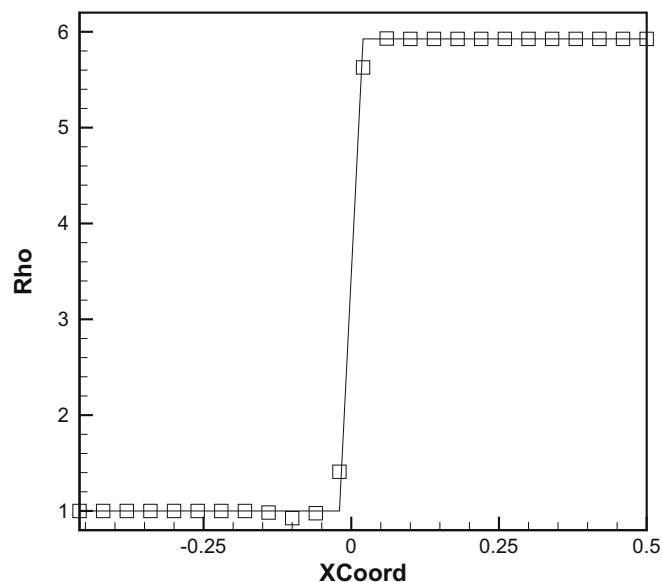


Fig. 17. Test 3 – EC1 flux plot of density at  $M_0 = 20.0$ .

$$\hat{\mathbf{D}}_{EC2} = (\hat{\mathbf{A}}_{EC2} + \alpha_{EC2} [|\mathbf{\Lambda}_{u \pm a}|]) \hat{\mathbf{S}} \tag{59}$$

adding a small dissipation to the acoustic waves of the upwinding term, producing additional entropy of  $O([\cdot]^2)$  with

$$\hat{\mathbf{A}}_{EC2} = \text{diag}((1 + \beta)|\hat{u} - \hat{a}|, |\hat{u}|, (1 + \beta)|\hat{u} + \hat{a}|) \tag{60}$$

where  $\beta = 1/6$  empirically determined to ensure the density is non-oscillatory without excessively smearing the shock profile. In addition, entropy is also produced at  $O([\cdot]^3)$  but with

$$\alpha_{EC2} = (\alpha_{max} - \alpha_{min})(\max(0, \text{sign}(dM_{max} - [M]))) + \alpha_{min} \tag{61}$$

where  $\alpha_{min} = 1/6$  and  $\alpha_{max} = 2.0$  (an approximate average value between 1.5 and 2.6).  $[M]$  is the change of Mach number at the flux interface. Finally  $dM_{max} = 0.5$  is empirically determined so that only the subsonic region of the shock is multiplied

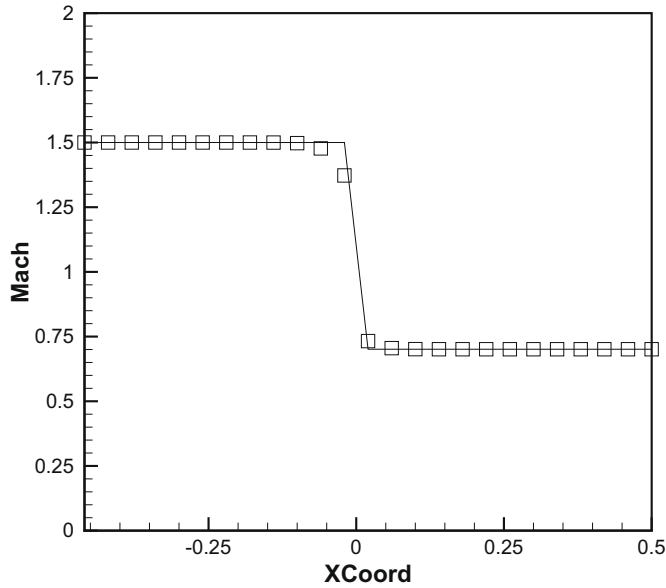


Fig. 18. Test 3 – EC2 flux with  $M_0 = 1.5$ .

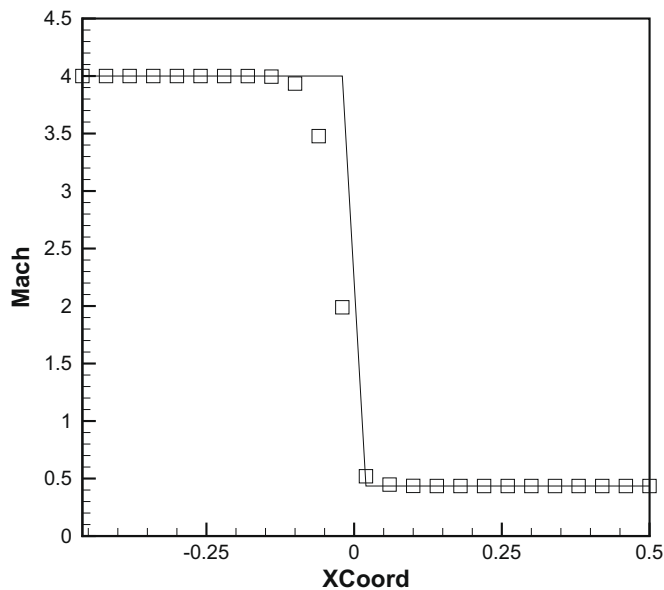


Fig. 19. Test 3 – EC2 flux with  $M_0 = 4.0$ .

with  $\alpha_{max}$  and overall produce a shock quality comparable to EC1 flux. This new dissipative matrix  $\hat{D}_{EC2}$  used in Eq. (41) will be referred to as EC2 flux in this paper.

The results of EC2 flux are shown in Figs. 18–22 indicating that there are no more under/overshoots for the density profile for  $M_0 = 20.0$  (Fig. 21) but in terms of Mach number, EC2 results are similar to the results of EC1.

It may seem that the EC1 (or EC2) flux is not conservative since the shock corresponding with the Mach number has moved upstream (Fig. 16). However, there is an explanation for this occurrence. Conservation only applies to the mass (Fig. 21), momentum and energy but the velocity is not conserved. As a result, the Mach number is also not conserved, resulting in a shift of its shock profile, with larger shifts for larger  $M_0$ .

Results using a second order high resolution method using Hancock scheme for EC2 fluxes (Figs. 22 and 23) are also included to show the captured shocks are ‘tighter’ compared to a first order method. Of course the Roe flux captures the stationary shocks exactly and the results are omitted for brevity.

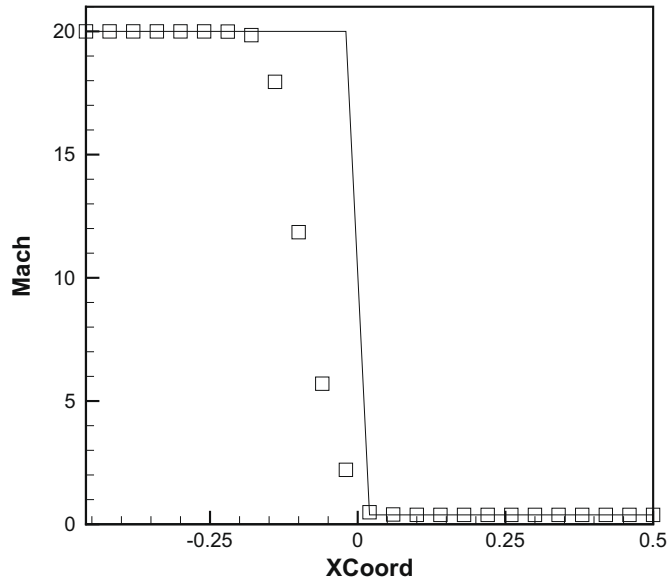


Fig. 20. Test 3 – EC2 flux with  $M_0 = 20.0$ .

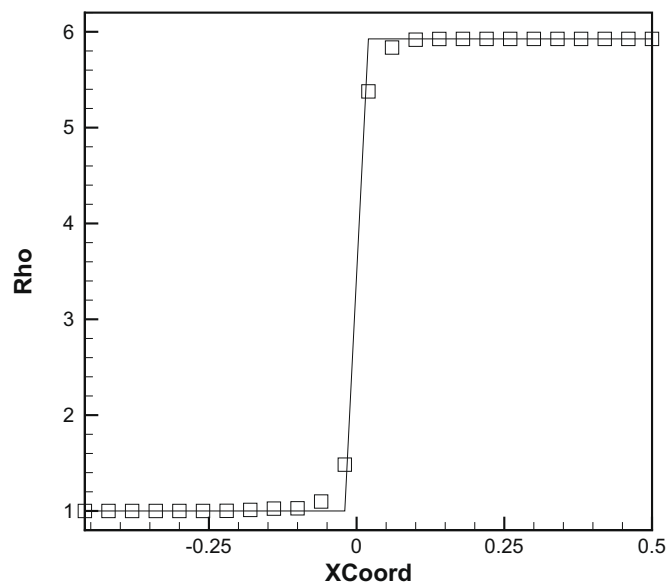


Fig. 21. Test 3 – EC2 flux plot of density at  $M_0 = 20.0$ .

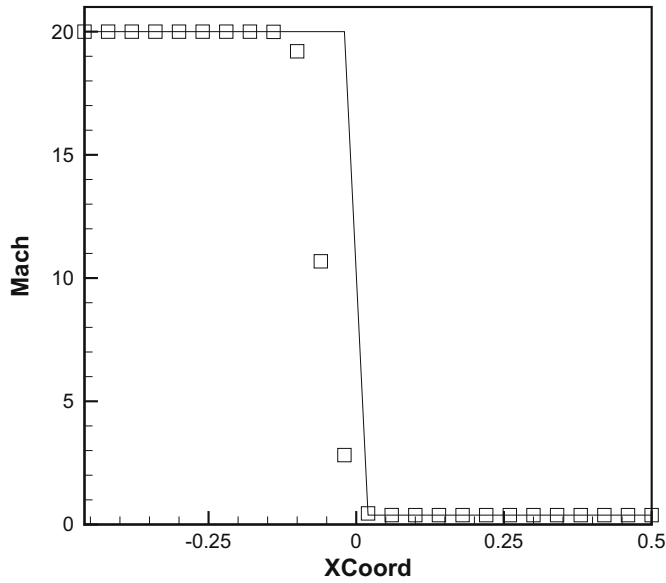


Fig. 22. Test 3 – EC2 (second order with Minmod) with  $M_0 = 20.0$ .

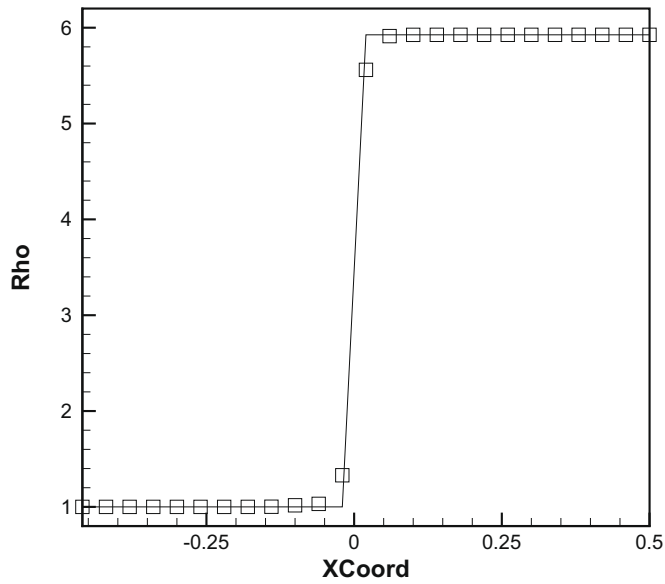


Fig. 23. Test 3 – EC2 (second order with Minmod) plot of density at  $M_0 = 20.0$ .

### 6.2. Test case IV: modelling a stationary contact

The following initial value problem is prescribed with zero slopes on the inflow and outflow where.

$$\rho_L = 10, \quad \rho_R = 1, \quad u_L = u_R = 0, \quad p_L = p_R = 1 \tag{62}$$

The new methods (ES, EC1 and EC2 fluxes) *exactly* preserve the contact discontinuity (Fig. 24). This also implies that the new flux function can predict boundary layers with minimal diffusion much like the Roe flux.

### 6.3. Test case V: modelling a rarefaction shock

This test is identical to modelling of the stationary shock except that it is just the *reversed* initial values of the Rankine–Hugoniot jump conditions. We have prescribed zero slopes at both the inlet and outlet boundaries.

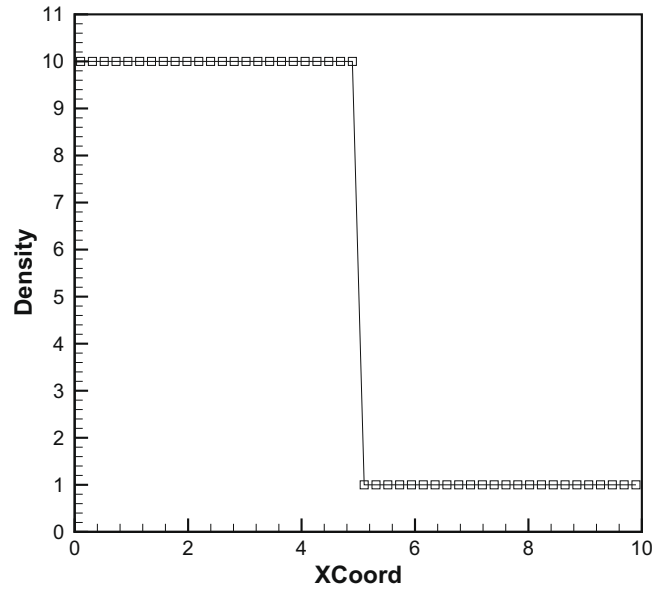


Fig. 24. Test 4 – Solution of Roe, ES and EC1 (and EC2) fluxes where contact is preserved exactly.

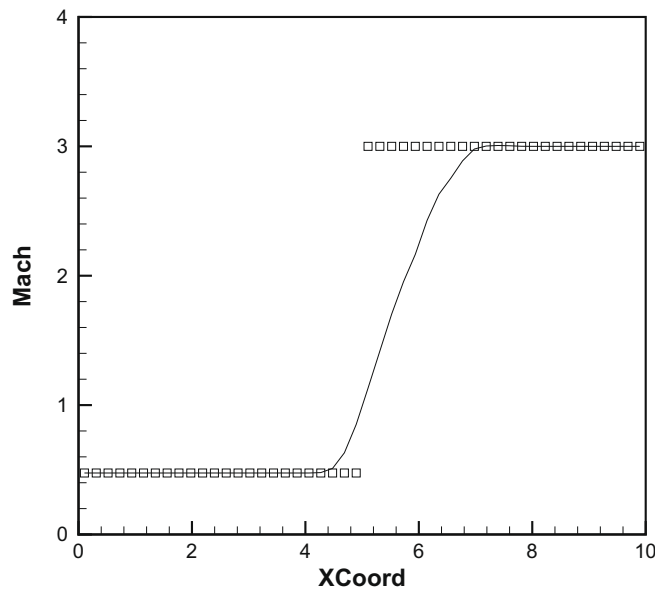


Fig. 25. Test 5 – Original Roe flux producing rarefaction shocks.

As shown in Figs. 26 and 27, the both of the new schemes predicts the rarefaction fan unlike the original Roe flux (Fig. 25). This is one of the positive outcome of including a more precise control of entropy. As expected, the EC2 (similar results for EC1) flux produces slightly smoother profile due to the extra dissipation. In addition, using a second order method produces an even more accurate prediction of the expansion region [5].

#### 6.4. Modelling Sod's shock tube problem

Up until this point, the EC flux function has only been tested for steady Euler problems. Now, we intend to demonstrate its ability to predict the unsteady Euler equations. We refer to Sod's problem where

$$p_L = 10^5, \quad \rho_L = 1.0, \quad u_L = 0.0 \tag{63}$$

$$p_R = 10^4, \quad \rho_R = 0.125, \quad u_R = 0.0 \tag{64}$$

utilizing 100 computational cells with  $\nu = 0.8$ . Results are shown at  $t = 0.0061$ .

The EC2 flux produces very similar results compared to those produced by the Roe flux (Figs. 28–31). For first order methods, results of the moving contact discontinuity are almost equivalent between the two flux functions, each capturing with about eight intermediate cells. However, EC2 flux captures the moving shock with five intermediate cells as opposed to four cells captured by the first order Roe flux. Second order solutions (using Hancock scheme with Superbee limiter) of both fluxes are almost identical, capturing the contact discontinuity with only four intermediate cells and the shock with only two intermediate cells.

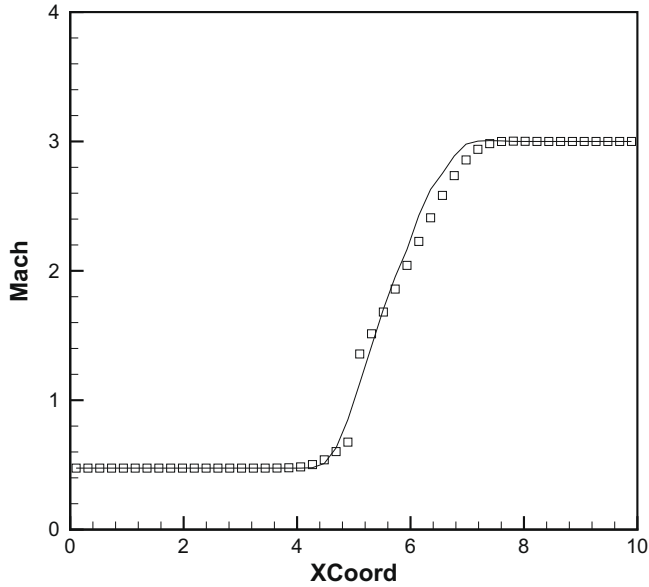


Fig. 26. Test 5 – ES flux correctly predicts the rarefaction fan.

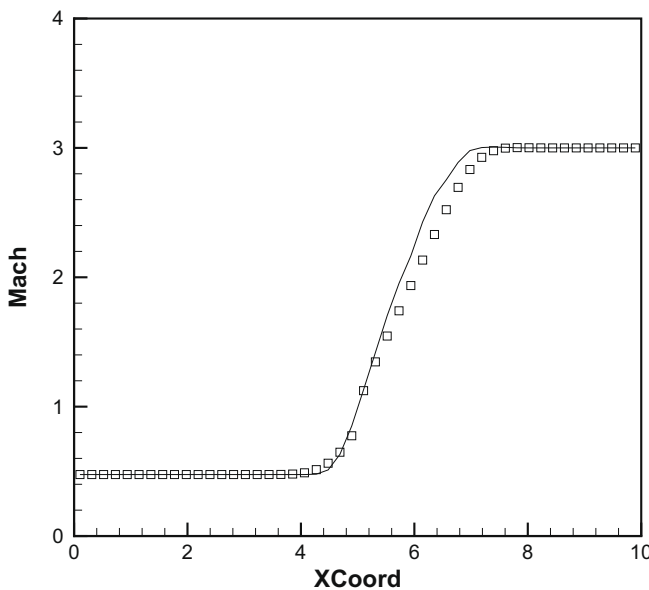


Fig. 27. Test 5 – EC2 flux adds some smoothing to the rarefaction fan.

### 6.5. Investigation of 1D shock instability

So far, we have shown that the EC2 flux captures shocks of any strength with reasonable success, in the sense that steady and unsteady shocks are captured with only a few intermediate cells. In this section, we intend to investigate if entropy consistency is enough to completely remove shock instability.

Shock instability which relates to the carbuncle phenomenon occurs when a blunt body is subjected to a strong shock, where the captured shock produces spurious solutions usually in the form of two counter rotating vortices near the stagnation region [11]. It is strongly suspected that instability arises from either round-off errors due to the grids or from the grids forcing the intermediate point(s) of a shock to be in a certain incompatible location. To mimic this in one dimension, Test III (Section 6.1) is used except that intermediate values are introduced within the shock satisfying

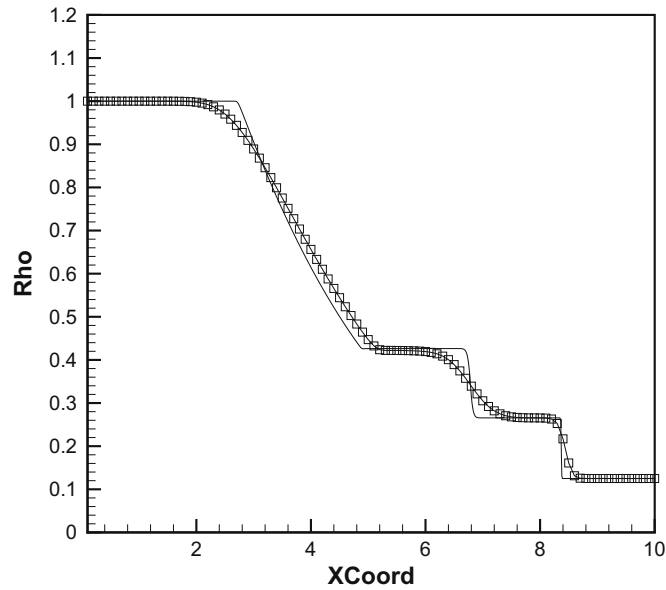


Fig. 28. Density plot of Sod's problem for Roe flux.

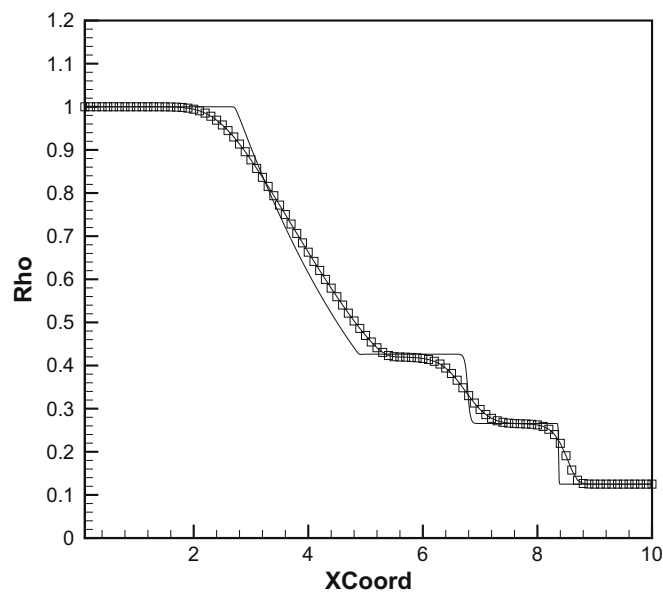


Fig. 29. Results of EC2 flux.

$$\mathbf{U} = \delta \mathbf{U}_0 + (1 - \delta) \mathbf{U}_1 \tag{65}$$

where  $\delta = 0.0, 0.1, 0.2, \dots, 1.0$ .

Note that the shock instability of a real blunt body problem has a certain stand-off shock position. To be consistent with this, the 1D shock location is not allowed to shift. Recall that for Test III, the outlet boundary conditions are based on a fixed mass flux with other fluxes being zero gradient. As a result, the total mass within the system is conserved hence restricting the shock (based on conservative variables) from shifting. However, the intermediate point(s) within the shock is(are) free to relocate, generating acoustic and entropy waves that are broadcasted downstream to the exit. Due to the nature of the exit, these waves are reflected back to the shock and force its intermediate points to relocate once more resulting a limit cycle

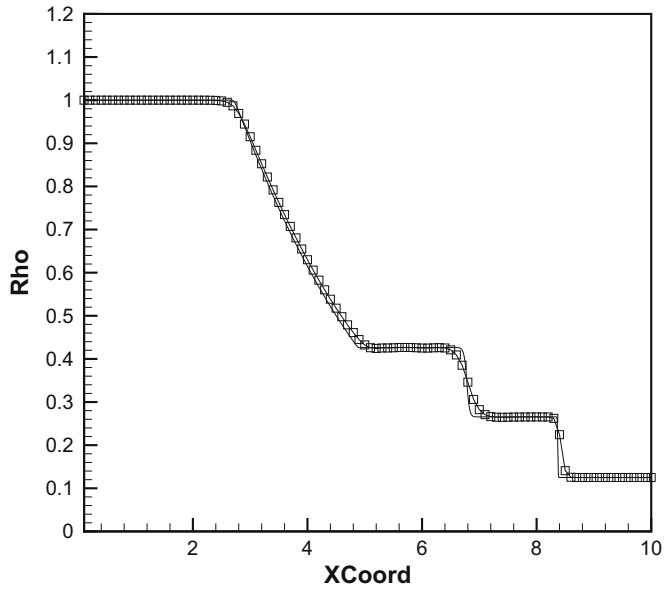


Fig. 30. Second order (superbee) limited Roe flux. The contact is now captured with only four intermediate cells.

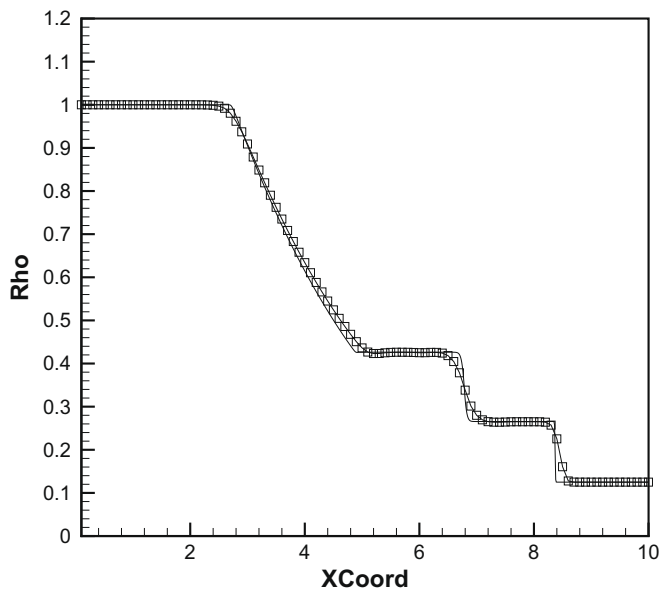


Fig. 31. Second order (superbee) limited EC2 flux. Almost identical to the second order Roe flux.

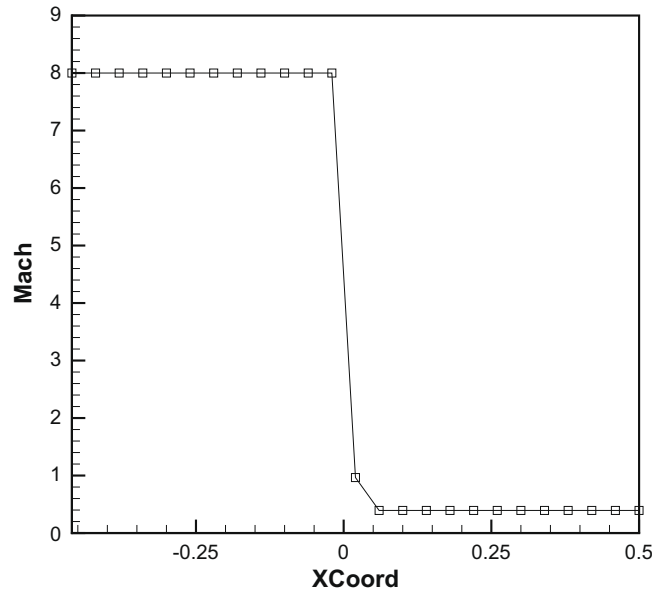


Fig. 32. 1D shock instability predicted by the original Roe flux at  $t = 0$  and  $t = 340$ .

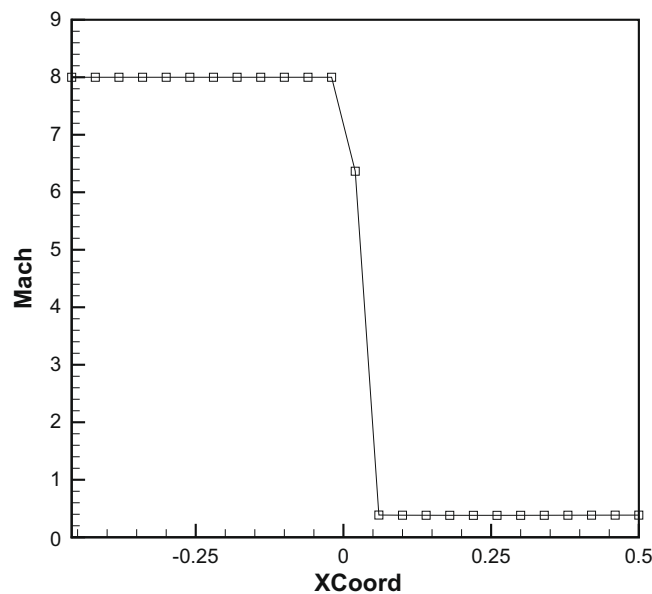


Fig. 33. The shock profile at  $t = 200$  and  $t = 680$ , demonstrating a limit cycle.

(Figs. 32 and 33). The shock instability usually occurs when using numerical flux functions that are minimally dissipative such as the original Roe flux. The residual of the Roe flux is plotted in Fig. 36, showing the solution does not converge even after 100,000 time-steps ( $t = 20,000$ ).

Our results indicate that the EC1 flux (which is not completely entropy-consistent) does not provide a complete range of 1D shock stability (Fig. 34), but has a smaller instability spectrum compared to the original Roe flux (Fig. 35). Kitamura et al. [6] used  $\alpha = 0.8$  to achieve full shock stability in 1D, but pointed out that this selection of  $\alpha$  causes the numerical solution to 'blow-up' in higher dimension. This behavior is similar to our numerical experiments in one dimension, where there is a limit to which  $\alpha$  can be increased before the solution 'blows-up'. However, our numerical results indicate that EC2 flux solution does not 'blow-up' in higher-dimensions and more importantly the shock is completely stable for all  $\delta$  in one dimension.

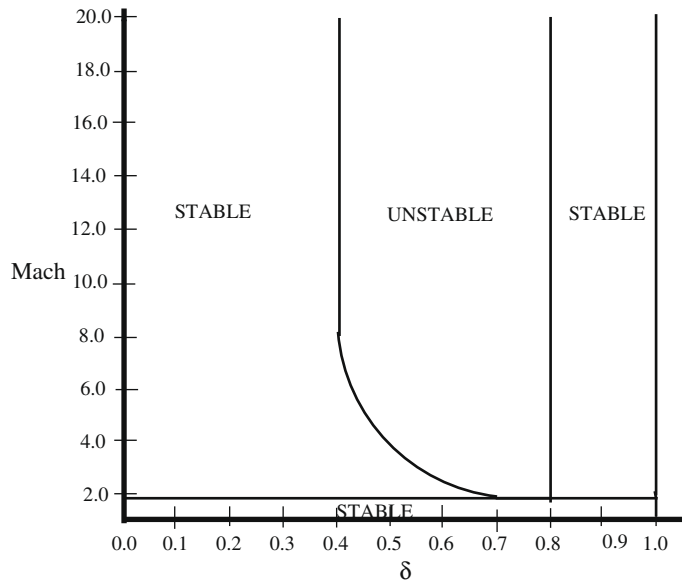


Fig. 34. 1D shock stability spectrum for the EC flux.

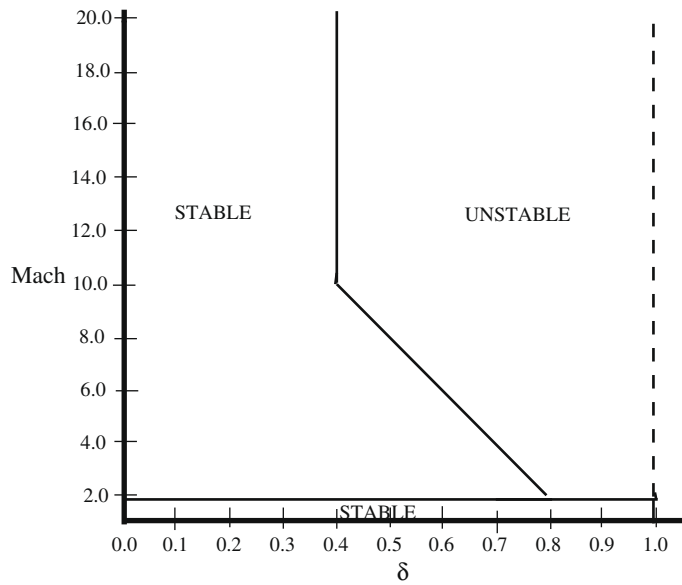


Fig. 35. 1D shock stability spectrum for the original Roe flux.

## 7. Concluding remarks

We have introduced into the numerical treatment of the conservation laws what may appear to be artificial terms in order to control the quality of captured discontinuities. Why should such terms be necessary?

It has been shown by Tadmor and Zhong [17] that stationary shocks can be captured by solving the Navier–Stokes equations with an entropy conserving Euler flux and central differences for the dissipation. However, to do this, they required an extremely fine grid. Without the dissipative terms, the solution was extremely oscillatory, as were the solutions with dissipation on coarse grids. In fact, the oscillations built up until they were strong enough to excite a commensurate response from the dissipation. On finer grids, the oscillations did not have to be so strong to do this, and eventually (on grids finer than any actually employed) the oscillations would disappear, because the true shock structure of the Navier–Stokes equations would be revealed.

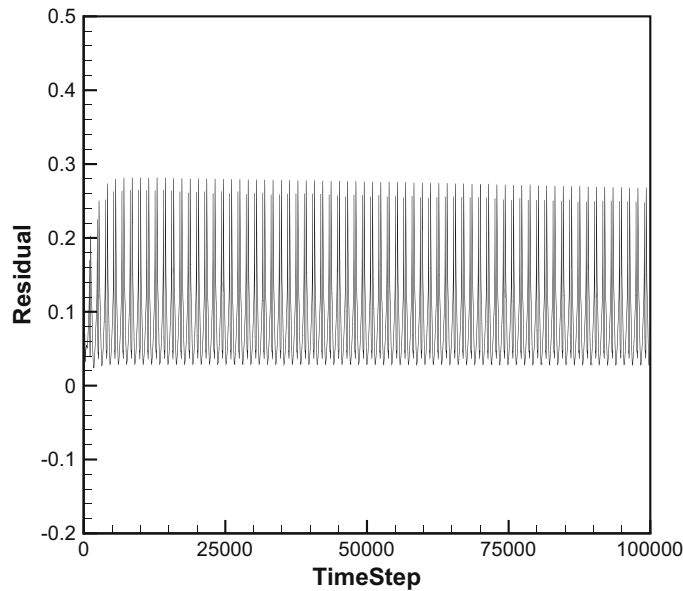


Fig. 36. The residual of an unstable 1D steady shock.

That would require, of course, that the grid be finer than the shock thickness, and probably less than the mean free path ( $O(10^{-6}m)$ ). For many calculations, the shock structure is of no interest, and a far coarser resolution is adequate. The terms that are added into the Euler equations here to yield entropy production can be thought of as subgrid terms that compensate for the lack of resolution.

If these subgrid terms are to be retained in a very fine grid shock calculation, they will decrease in importance as the grid is refined. They produce entropy proportional to the square and cube of the difference in states, which is larger for an under-resolved shock, but small for a resolved shock. On the contrary, the physical dissipation terms produce entropy proportional to only the square of the difference in states, although multiplied by very small coefficients.

Results of the entropy-consistent flux (EC2) imply that one dimensional entropy consistency provides complete shock stability in one dimension. However it is still unclear at this stage whether one dimensional entropy consistency will guarantee shock stability in higher-dimensions. Perhaps the concept of one dimensional entropy consistency must be coupled with some form multidimensional dissipation mechanism as proposed by Nishikawa and Kitamura [9], Roe and Kitamura [13] to achieve full 2D and 3D shock stability. This will be left as an avenue for future work. Overall, we hope that the principles of entropy consistency in this paper will serve to better understand from a physical basis on how to completely remove shock instability and eventually the carbuncle phenomenon.

### Acknowledgments

This research was supported in part by Universiti Sains Malaysia RU grant and by Space Vehicle Institute under Grant NCC3-989, one of NASA University Institutes, University of Michigan Department of Aerospace Engineering.

### Appendix A. Entropy conserving flux

The entropy conserving flux [16] satisfies

$$\mathbf{v}^T \mathbf{f}_c = [\rho \mathbf{u}] \quad (66)$$

and is explicitly computed as averaged quantities of

$$\mathbf{f}_c(\mathbf{u}_L, \mathbf{u}_R) = \begin{bmatrix} \hat{\rho} \hat{u} \\ \hat{\rho} \hat{u}^2 + \hat{p}_1 \\ \hat{\rho} \hat{u} \hat{H} \end{bmatrix} \quad (67)$$

We now determine these averaged states. Define

$$z_1 = \sqrt{\frac{\hat{\rho}}{\hat{p}}}, \quad z_2 = \sqrt{\frac{\hat{\rho}}{\hat{p}}} u, \quad z_3 = \sqrt{\hat{\rho} \hat{p}} \quad (68)$$

so that the averaged quantities are computed as functions of arithmetic mean ( $\bar{a} = \frac{a_L + a_R}{2}$ ) and logarithmic mean (defined in Appendix B). Choose  $\hat{u} = \frac{\bar{z}}{z_1}$  and insert into Eq. (66) to obtain

$$\hat{\rho} = \bar{z}_1 z_3^{\ln} \tag{69}$$

$$\hat{p}_1 = \frac{\bar{z}_3}{z_1} \tag{70}$$

$$\hat{p}_2 = \frac{\gamma + 1}{2\gamma} \frac{z_3^{\ln}}{z_1^{\ln}} + \frac{\gamma - 1}{2\gamma} \frac{\bar{z}_3}{z_1} \tag{71}$$

$$\hat{a} = \left( \frac{\gamma \hat{p}_2}{\hat{\rho}} \right)^{\frac{1}{2}} \tag{72}$$

$$\hat{H} = \frac{\hat{a}^2}{\gamma - 1} + \frac{\hat{u}^2}{2} \tag{73}$$

**Appendix B. Logarithmic mean**

Let  $a$  be some quantity of interest which has a left and right state. The logarithmic mean of  $a$  is defined as

$$a^{\ln}(L, R) = \frac{a_L - a_R}{\ln(a_L) - \ln(a_R)} \tag{74}$$

However, this is not numerically well-posed when  $(a_L) \rightarrow (a_R)$ . To overcome this, let us write the logarithmic mean in another form. Let  $\zeta = \frac{a_L}{a_R}$ , so that

$$a^{\ln}(L, R) = \frac{a_L + a_R}{\ln \zeta} \frac{\zeta - 1}{\zeta + 1} \tag{75}$$

where  $\ln(\zeta) = 2 \left( \frac{1 - \zeta}{1 + \zeta} + \frac{1}{3} \frac{(1 - \zeta)^3}{(1 + \zeta)^3} + \frac{1}{5} \frac{(1 - \zeta)^5}{(1 + \zeta)^5} + \frac{1}{7} \frac{(1 - \zeta)^7}{(1 + \zeta)^7} + O(\zeta^9) \right)$

to obtain a numerically well-formed logarithmic mean. The subroutine for computing the logarithmic mean is the following. Let

$$\zeta = \frac{a_L}{a_R}, \quad f = \frac{(\zeta - 1)}{(\zeta + 1)}, \quad u = f * f$$

1. if  $(u < \epsilon)$

$$F = 1.0 + u/3.0 + u * u/5.0 + u * u * u/7.0$$

2. else

$$F = \ln(\zeta)/2.0/(f)$$

so that  $a^{\ln}(L, R) = \frac{a_L + a_R}{2F}$  with  $\epsilon = 10^{-2}$ .

**References**

[1] J.D. Anderson, Modern Compressible Flow with Historical Perspective, second ed., Springer, 2004.  
 [2] T.J. Barth, An introduction to recent developments in theory and numerics of conservation laws, Num. Methods Gasdynamic Syst. Unstructured Meshes (1999).  
 [3] M. Dumbser, J.M. Moschetta, J. Gressier, A matrix stability analysis of the carbuncle phenomenon, J. Comput. Phys. 197 (2004) 647.  
 [4] T. Hughes, L. Franca, M. Mallet, A new finite element formulation for compressible fluid dynamics: I. Symmetric forms of the compressible Euler and Navier–Stokes equations and the second law of thermodynamics, Comput. Methods Appl. Mech. Eng. 54 (1986).  
 [5] F. Ismail, Toward a reliable prediction of shocks in hypersonic flow: resolving carbuncles with entropy and vorticity control, Ph.D. Thesis, The University of Michigan, 2006.  
 [6] K. Kitamura, P.L. Roe, F. Ismail, An evaluation of Euler fluxes for hypersonic computations, no. 2007-4465, AIAA Conference, 2007.  
 [7] C. Laney, Computational gasdynamics, 1998.  
 [8] P.D. Lax, Hyperbolic systems of conservation laws and the mathematical theory of shock waves, in: SIAM Regional Conference Series in Applied Mathematics, 1972.  
 [9] H. Nishikawa, K. Kitamura, Very simple, carbuncle-free, boundary-layer-resolving, rotated-hybrid Riemann solvers, J. Comput. Phys. 227 (2008) 2560–2581.  
 [10] S. Osher, Riemann solvers, the entropy condition and difference approximations, SIAM 21 (1984) 217–235.  
 [11] M. Pandolfi, D. D'Ambrosio, Numerical instabilities in upwind methods, J. Comput. Phys. 166 (2001) 271–301.

- [12] J.J. Quirk, A contribution to the great Riemann solver debate, *Int. J. Num. Methods Fluids* 18 (1994) 555–574.
- [13] P.L. Roe, K. Kitamura, Artificial surface tension to stabilize captured shockwaves, no. 2008-3991, AIAA Conference, 2008.
- [14] P.L. Roe, Approximate Riemann solvers, parameter vectors and difference schemes, *J. Comput. Phys.* 43 (1981) 357–372.
- [15] P.L. Roe, Sonic flux formulae, *SIAM J. Sci. Stat. Comput.* 13 (1992) 611–630.
- [16] P.L. Roe, Affordable, entropy-consistent, Euler flux functions I. Analytical results, *J. Comput. Physics*, submitted for publication.
- [17] E. Tadmor, W. Zhong, Entropy stable approximations of Navier–Stokes equations with no artificial numerical viscosity, *J. Hyperbolic DE's* (2005).